Recent Topics on High Field Magnetism in Low Temperatures

Taturu YOSIDA and Muneyuki DATE*

Low Temperature Center, Osaka University, Toyonaka, Osaka 560,
and Department of Electronic Mechanical Engineering, Nakanihon Automotive College,†
Sakahogi-cho, Gifu 505, Japan
*Department of Science, Faculty of Science, Osaka University, Toyonaka, Osaka 560, Japan

Abstract: The experimental facilities in the High Magnetic Field Laboratory of Research Center for Extreme Materials, Osaka University, are extended below 1 K by introducing ^{3}He cryostat in the large-bore pulsed magnet system (maximum field 40T). The details of the magnetization measuring system are shown. The system has been successively applied to magnetization measurements of Cr trinuclear compounds showing the ground-state crossover phenomenon and those of the so-called Haldane compounds with the excitation energy gaps.

1. INTRODUCTION

Magnetization measurements of magnetic materials under a high magnetic field in the low temperature regions serve as a very useful tool for investigating the magnetic interactions. In the High Magnetic Field Laboratory of Research Center for Extreme Materials, Osaka University, measurement systems using liquid helium down to 1.3 K has been established and many interesting experimental results have been reported. [1, 2] However, some samples have their ordered state below or near liquid helium temperature and investigations in the temperature region below 1 K are often required. Electrical resistivity measurements below 1 K have been sometimes requested for metals and alloys in connection to the superconductivity.

A ^{3}He cryostat system has been introduced in order to extend the experimental facilities to lower temperatures. The lowest temperature achieved is 0.5 K even in the pulsed magnetic field as high as 400 kOe (40 T). The apparatus described below is employed satisfactorily for magnetization measurements under these conditions. The similar cryostat

† : Permanent address from Oct. 1992.

is also developed for another magnet with pulse width about 100 times longer. The details of apparatus mainly for the former magnet system and some experimental topics obtained by the cryostat are shown in section 2 and section 3.

2. APPARATUS

2. 1 Pulsed Magnet

There are two kinds of the field generation systems in the Laboratory with the capacitor bank of 0.5 and 1.25 MJ, respectively. [1] The magnets for both energy sources consist of multi-layer coils which are designed so as to share strong Maxwell stress within their tensile strength. The former energy source is used for the Long Pulse Magnet System which can supply magnetic field up tp 400 kOe in a space of 16 mm in diameter with the pulse width of about 30 ms and the latter one, the Short Pulse Magnet System, produces a field up to 700 kOe with 18 mm in diameter with pulse width of 0.3 ms.

Three types of the magnets are available for practical use. Their sizes and characteristics

Table 1. Magnet characteristics

Magnet type		"Short Pulse"		"Long Pulse"
		150(1L)60*1	150(2L)20	170(2LP)18
Coil				
type		1 layer	2 layer	2 layer
outer diameter	(mmϕ)	150	50*2	170 80*3
inner diameter	(mmϕ)	60	20*2	84 18*3
length	(mm)	80	60*2	130 100*3
windings		single	single	multi
	(turns)	12	5*2	491 222*3
wire cross-section (mm × mm)		5 × 45	8 × 15*2	2 × 4
inductance	(μH)	6	7*2	17.5 mH
resistance	(mΩ)	20	30*2	175
Capacitor Bank		D-2 1.25MJ	D-2 1.25MJ	D-1 0.5MJ
Rating				
max. field	(T)	50	70	40
pulse width	(msec)	0.35	0.35	30
effective bore	(mmϕ)	58	18	16
inner dia. of He dewar	(mmϕ)	26	6	10
repetition rate	(hr^{-1})	2	2	2

* 1 notation: *outer diameter* (*number of Layers*) *inner diameter*. LP stands for "Long Pulse".

* 2 These value are for the inner coil. The size of the outer coil is same as that of one-layer coil 150 (1L)60.

* 3 The values in the left are for the outer coil and those in the right for the inner one.

are listed in Table 1. The intensity of the magnetic field is detected by using pick-up coils and calibrations of the coils are accomplished by the method of ESR with the FIR laser. This method allows the accuracy of field intensity measurements to be ± 0.3 %.

The cross-sectional view of the two-layer 'Short Pulse' magnet 150(2L)20 is shown in Fig. 1. The inner-layer coil and the outer-layer coil are connected electrically in series and pulsed current is provided with 24 coaxial cables. Pulsed current flows through the shaded area of the magnet. The magnet is operated at room temperature and dewar vessel with a sample is inserted into the magnet. The magnet filed distribution along the axis of the magnet is also shown in Fig. 1. The field A (or B) is produced when only the inner coil "a" (or outer coil "b") is operated and the field A+B is generated when both "a" and "b" coils are operated cooperatively.

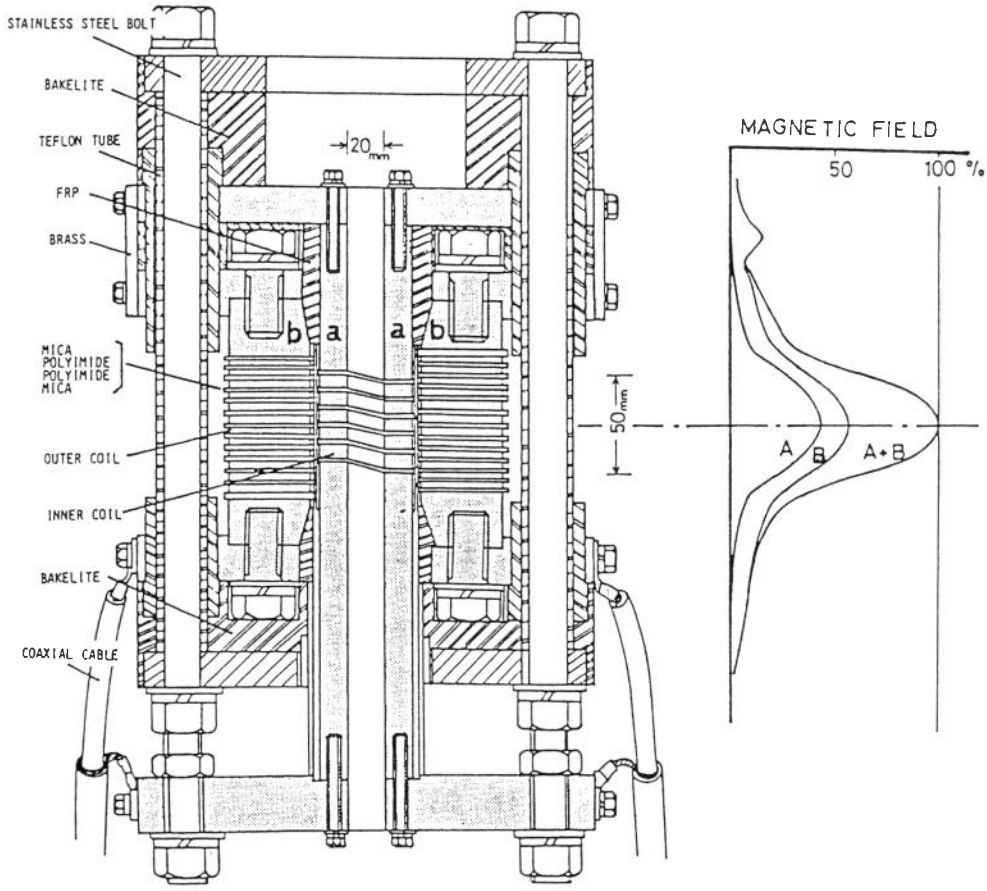

Fig. 1. Cross-sectional view of the two-layer magnet and the field intensity distribution on the axis of the magnet.

The 'Long Pulse' magnet consists of two-layer magnets which are multi-winding so as to obtain a large inductance. This magnet is operated immersed in liquid nitrogen to reduce electric resistance. Because the pulse duration is longer, the metallic parts such as waveguides made of cupric nickel (German silver)for microwave propagation are available without severe heating due to eddy currents.

3. 2 ^{3}He cryostat

A conventional single-shot type ^{3}He cryostat has been developed for the magnetization measurements. [3] The cut view of the cryostat with the magnet location is illustrated in Fig. 2. The magnet is 150(1L)60, *i. e.* a single layered magnet with an inner diameter of 60

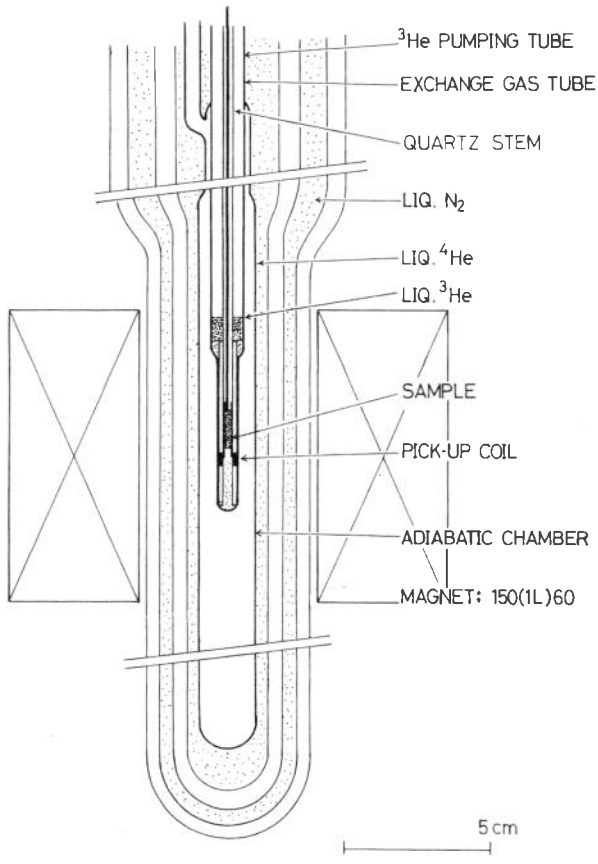

Fig. 2. Cut view of ^{3}He cryostat for magnetization measurements.

mm and maximum field of 400 kOe (only "b" coil in Fig. 1). Such a large magnet enables us to perform the experiments below 1K. The dewer vessels are made of glass with partially silver plating to avoid the skin effect and eddy current heating due to the pulsed field.

The sample is mounted on the end of teflon tube (3mm in outer diameter) with a teflon holder and best position is adjusted by this teflon tube. The two-turn field-pick-up coil is wound outside of the adiabatic chamber and the magnetization-pick-up coils are wound on the Bakelite bobbin, as shown in Fig. 3, which is set immmersed in the ^{3}He chamber and supported from the top flange by Bakelite pipe and quartz pipe.

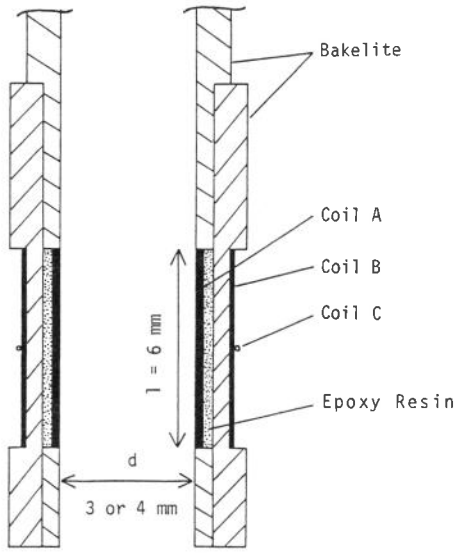

Fig. 3. Cut view of magnetization pick-up coil.

The technically important point of the magnetization-pick-up coil system is how to compensate the background flux change due to a transient field. This is done by setting three coils as shown schematically in Fig. 4(a). [5] Coil 'A' (about 100 turns) pick up the magnetic flux change of the sample while the coil 'B' (about 50 turns) is wound in the opposite direction with respect to 'A' in order to compensate the background flux change. The cross section of B-coil is twice as large as that of A-coil so as to make the net flux in A-coil is equal to that in B-coil. Fine adjustment is done by adjusting the output from the one-loop coil 'C' using bridge balance circuit as shown in Fig. 4 (b). The output signal of the bridge balance circuit is proportional to dM/dt but still contains background noise. The transient digital recorder is used to reduce this residual noise. Two sets of data, with and without specimen, are taken by using two shots of pulsed field. The signal dM/dt is obtained by the difference of these two data. The field derivative of magnetization dM/dH is calculated by dividing the subtracted data dM/dt by the signal dH/dt. The field and magnetization pick-up coil are calibrated by single crystalline MnF_2 as the standard specimen using its spin-flop transition field and the susceptibility above the transition.

The exchange gas chamber, as well as the dewar vessels, is silvered along the inside wall with two vertical slits of about 5 mm wide. The slits are necessary to cut the current loop

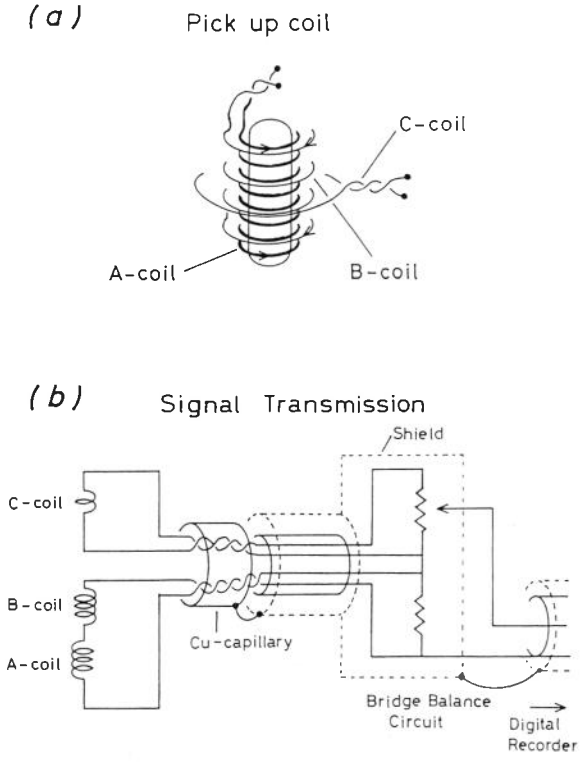

Fig. 4. Schematic view of the pick-up coil winding and the bridge balance circuit for the fine compensation.

along the wall. However, they cause heat inflow of about 80 μW to the liquid ^{3}He due to light. The volume of liquid ^{3}He is about 4 cm^3 and an experiment in 4-5 hours can be done after a condensation of ^{3}He under usual conditions.

Figure 5 shows the diagram of the pumping and storage system to handle the ^{3}He and exchange gas (^{4}He). The ^{3}He gas is pumped with a hermetically sealed rotary pump (DAIA CRP-100S), with a pumping speed of 100l/min. The turbo-molecular pump (BALZERS PFEIFFER TSU-100) is introduced to obtain high vacuum in exchange gas chamber in a short period after ^{3}He is condensed. Vacuum of 2×10^{-6} Torr (2.7×10^{-4} Pa) is obtained in 15 minutes. The temperature of ^{3}He bath is controlled by regulating the vapor pressure, which is measured by diaphragm vacuum gauge (BARATRON) and the McLeod gauge through the tube connected to the sample.

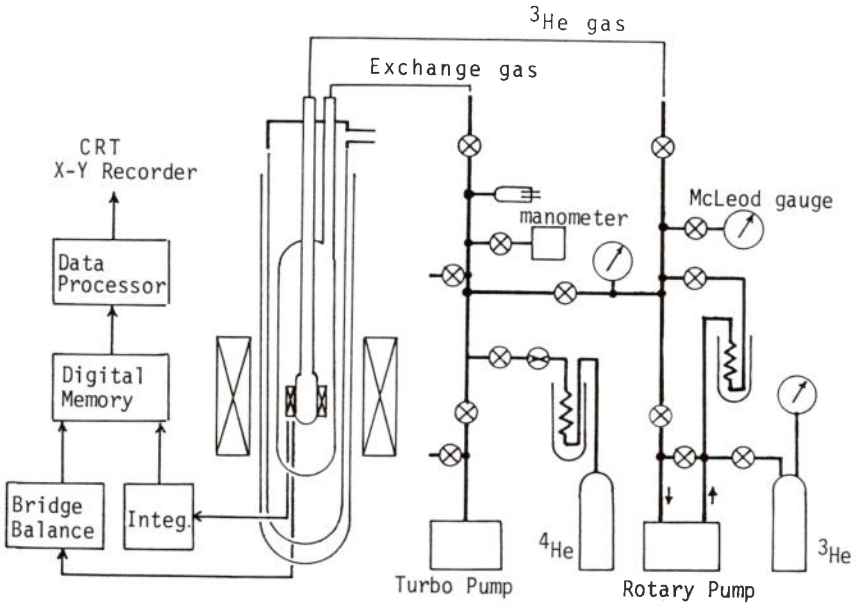

Fig. 5. Schematic diagram of ^{3}He cryostat and gas handling system. A Kenny pump to reduce the temperature of ^{4}He bath not shown. The diagram on the left side shows the data-processing system for magnetization measurements.

3. EXPERIMENTAL RESULTS BELOW 1 K

There are several experimental studies for which the measurements below 1 K are very effective. One of them is the observation of magnetization curves. The smoothing effect due to finite temperature sometimes prevents clear observations of the steps. In these cases, it is necessary to cool the samples down to lower temperatures beyond the conventional temperature of 1 K or higher. Experimental results of chromium-ion trimers [4] and Haldane compounds [6] performed below 1 K are illustrated as typical examples.

3. 1 Ground State Crossover in Cr-trinuclear Compounds

3. 1. 1. Introduction

Much work has been done experimentally and theoretically on the magnetic properties of chromium complexes containing Cr^{3+}-ion trimer. One of them is $[Cr_3O(CH_3COO)_6(H_2O)_3]\ Cl\cdot 6H_2O$, which is hereafter called Cr-acetate. Another is Cr-propionate with the chemical formula of $[Cr_3O(C_2H_5COO)_6(H_2O)_3]\ NO_3\cdot 2H_2O$. In these complexes three chromium ions are clustered together through a triply bridging oxygen ion

but widely separated from all other chromium triads in the crystal. [7, 8] In 1928, Welo reported the paramagnetic susceptibility in the temperature range from 200 to 300 K with the Curie-Weiss constant of − 93 K for Cr-acetate. [9] Kambe in 1950 introduced the exchange coupled trimer model where the antiferromagnetic exchange interactions between ions in a trimer are assumed to be equal. [10] In 1954, Wucher *et al.* [11] extended the measurement of the susceptibility down to liquid-helium temperature and proposed a model that the trimer is not equilateral but isosceles as is schematically shown in the insert in Fig. 7. The exchange Hamiltonian is written by

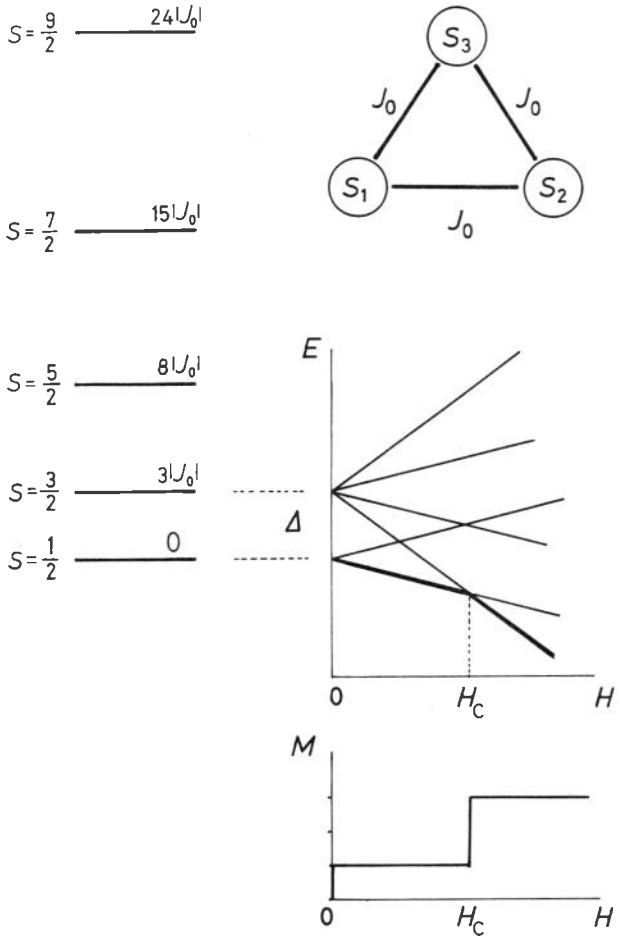

Fig. 6. Exchange coupling of equilateral trimer model. The energy levels, the ground-state crossover due to Zeeman splitting and magnetization curve at zero temperature are schematically shown.

$$\mathcal{H} = -2J_0(S_1S_2 + S_2S_3 + S_3S_1) - 2J_1S_1S_2, \tag{1}$$

where S_1, S_2 and S_3 are the Cr^{3+} spins of $S=3/2$, the exchange coupling parameter J_0 is negative and $|J_1/J_0| \ll 1$. The exchange parameters in Cr-propionate are estimated to be $J_0=-13.5$ K and $J_1=-1.9$ K by the optical measurement done by Morita *et al.* [12]

The schematic energy level diagram of the trimer spin system is given in Fig. 6, where J_1 is neglected for simplicity. Detailed level structure with J_1 for the ground and the first excited state is shown in Fig. 7. The ground state of the trimer is the spin doublets ($S=1/2$) reflecting the antiferromagnetic interactions between spins and the first excited states of $S=3/2$ lies $3|J_0|$ above the ground state. In a strong magnetic field, therefore, the ground-state crossover is expected at H_c as shown in Fig. 6. This phenomenon can easily be detected in the magnetization measurement because the magnetic moment below H_c is one

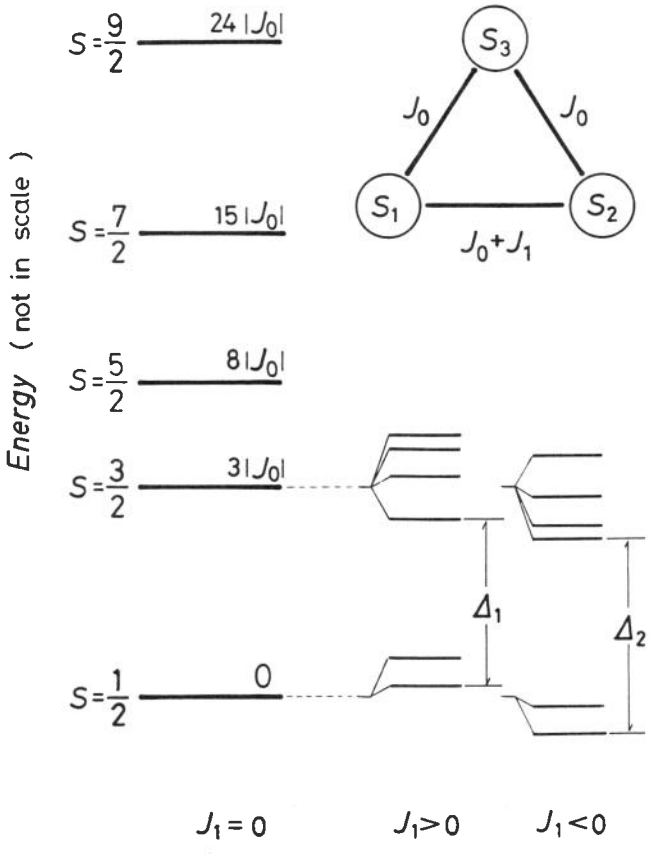

Fig. 7. Energy level splitting due to J_1 term and energy gaps.

Bohr magneton while the moment above H_c is three times larger than the low field value. The energy gap Δ between the ground and lowest excited state is thus obtained by accurate determination of H_c.

The increase in the magnetization at $T=0$ should be sharp, *i. e.*, an abrupt magnetization step is expected at H_c as shown in Fig. 6. At finite temperatures, however, the step is broadened due to thermal population of the spins and clear observation of the step is prevented. Therefore, it is necessary to cool the specimen down to lower temperatures beyond the conventional liquid helium temperature of 1 K in order to obtain the precise value of H_c.

3. 1. 2. Energy levels and results

The energy levels given by the exchange Hamiltonian of eq. (1) are calculated as [13]

$$E(S,\ S')=J_0\{45/4-S(S+1)\}+J_1\{15/2-S'(S'+1)\}, \tag{2}$$

where $S=S_1+S_2+S_3$ and $S'=S_1+S_2$. The magnitudes of gaps Δ_1 and Δ_2 in Fig. 7 are calculated from eq. (2) as

$$\begin{aligned} \Delta_1&=3\,|J_0|-6\,|J_1| \quad \text{for } J_1>0,\\ \Delta_2&=3\,|J_0|-2\,|J_1| \quad \text{for } J_1<0. \end{aligned} \tag{3}$$

In case of Cr-propionate ($J_1<0$), the value of gap is calculated to be $\Delta_2=36.7$ K. [12] At sufficiently low temperature, almost all spins occupy the ground level. Then the energy-level crossing which is related to the stepwise increase in the magnetization occurs at the critical field H_c given by,

$$g\mu_B H_c=\Delta_2 \tag{4}$$

The magnetization curves of Cr-propionate is shown in Fig. 8(a). The ordinate is expressed in unit of the Bohr magneton per trimer. The initial stage of the magnetization process up to about 80 kOe corresponds to the paramagnetic saturation of the ground state doublet. A large hysteresis for increasing and decreasing curves is observed in the low temperature region. It is attributed to the magnetocaloric effect, which acts as exothermic in the increasing field while it is endothermic in the decreasing one.

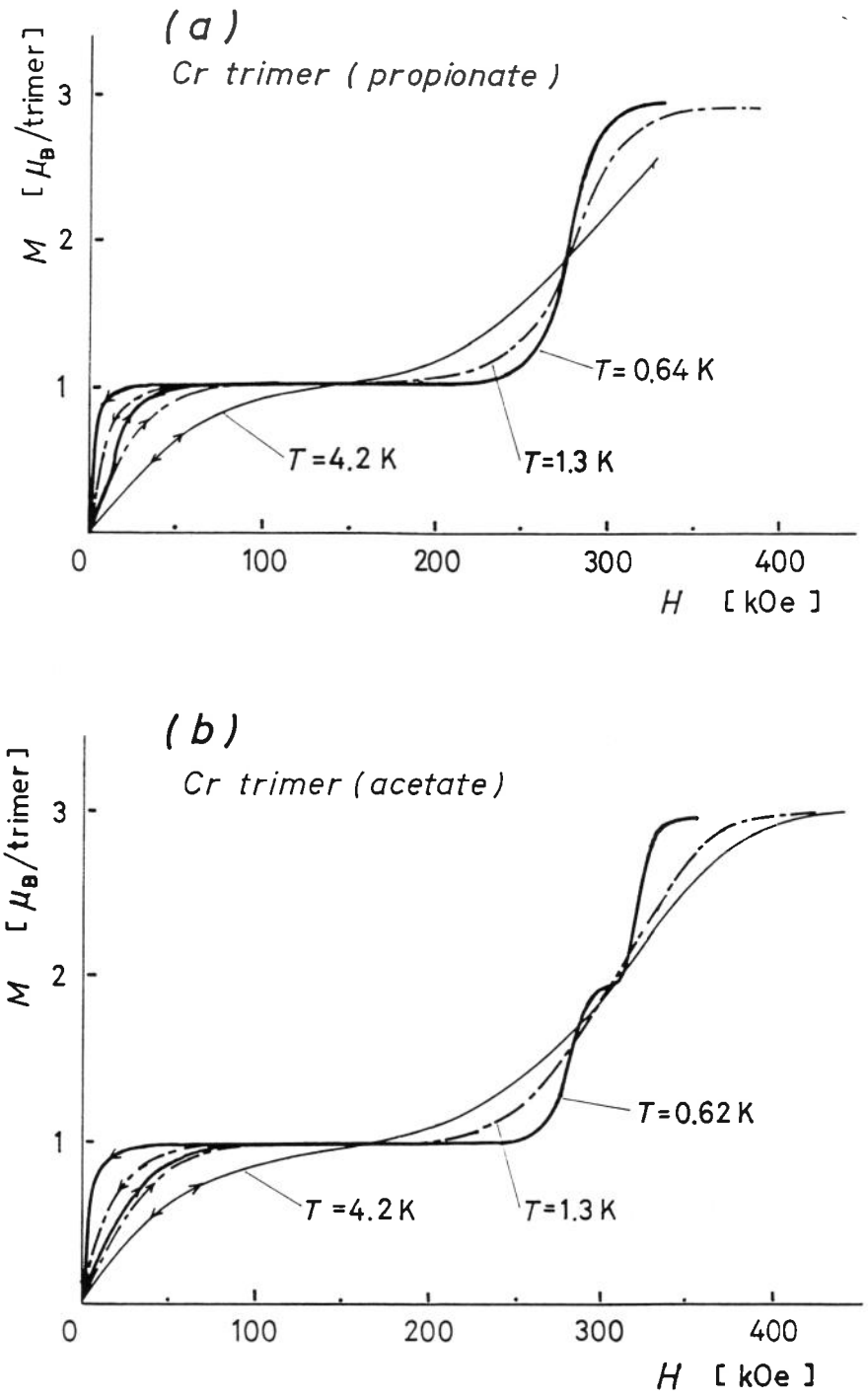

Fig. 8. Magnetization curves of (a) propionate Cr-trimer with one kind of trimer and (b) acetate Cr-trimer with two kinds of trimers.

The magnetization increase due to ground-state crossover is observed at $H_C = 272 \pm 4$ kOe and becomes steep as temperature decreases. It should be noted that the crossover field H_C is able to be precisely determined from the sharp maximum peak in dM/dH curve obtained at the lowest temperature of 0.6 K. The hysteresis around H_C is hardly observed. The energy gap Δ_2 is obtained as 36.7 ± 0.5 K by assuming $g = 2.0$. The energy gap agrees well with the optical data of 36.7 K.

On the other hand, Cr-acetate has been suggested to have two (equimolar) dissimilar trimers in low temperatures. The corresponding gaps are estimated to be 37.9 K and 43.8 K and the magnetization curve is expected to give two-step increase at H_{C1} and H_{C2}. The experiments performed only below 1 K could reduce the line bloadening effect and reveal the two-step increase, as shown in Fig. 8(b). However, the details of the experiment and analysis are given elsewhere [4] because of the length of this article.

3. 2 Haldane gap in $S=1$ linear antiferromagnets

3. 2. 1. Introduction

There has been an increasing interest in the spin wave energy spectrum of the one-dimensional Heisenberg antiferromagnet. In 1983, Haldane predicted that the one-dimensional Heisenberg antiferromagnet with integer spin value has an energy gap between the singlet ground state and the first excited one while the system with a half-integer spin value has no energy gap. [14] In the case of spin $S=1/2$, the eigen state energy was calculated exactly by Bethe using so-called the Bethe ansatz method.[15] No energy gap exists above the ground state. Magnetization and susceptibility curves have been calculated by Bonner and Fisher [16] and corresponding much experimental work has been accumulated. The one-dimensional Heisenberg antiferromagnet system has been believed to have no energy gap irrespective of the spin value.

The prediction by Haldane is now well supported theoretically by numerical calculations and exactly solvable model. [17] The value of this energy gap E_g in one-dimensional Heisenberg antiferromagnet with $S=1$ with following exchange Hamiltonian:

$$\mathcal{H} = -J \sum_j S_j S_{j+1}, \tag{5}$$

has been estimated numerically by Monte Carlo method to be $E_g = 0.41 \mid J \mid$. [18]

The presence of the uniaxial anisotropy (DS_Z^2) is inevitable for $S \geqq 1$ systems. Furthermore, the interchain exchange interaction (J')always exist in real materials. Botet *et al.*

[19] have done a finite-size-scaling study of the $S=1$ one-dimensional Heisenberg antiferromagnet with D-term. The lowest excited state they considered is triplet, which corresonds to an excitation with total spin 1 from the ground state. The excited triplet splits into a doublet and a singlet due to the D-term. An effect of single ion anisotropy term DS_Z^2 on the Haldane gap has been considered and it has been shown that the Haldane gap exists for $-0.29<D/|J|<0.93$. Moreover, Haldane gap is also stable when the interchain exchange interaction is small. [20]

$CsNiCl_3$ was first tried to observe the Haldane gap. Buyers *et al.* [21] and Steiner *et al.* [22] have done neutron scattering measurements and suggested that their experimental results support the existence of the Haldane gap. However, the interchain exchange interaction J' is not negligible in comparison with the intrachain exchange interaction J in this compound ($T_N=4.9$ K), so that it is difficult to observe the ideal Haldane state at enough low temperature.

Renard *et al.* have found several organic compounds which contain Ni^{2+} chains and have done suscetibility [23, 24] and neutron scattering [23—26] measurements on single crystal samples NENP and NINO with the chemical formulas $Ni(C_2H_8N_2)_2NO_2(ClO_4)$ and $Ni(C_3N_{10}N_2)_2NO_2(ClO_4)$, respectively. These compounds show no long-range magnetic order down to 0.5 K reflecting negligible interchain exchange interaction and regarded as suitable materials for testing the Haldane gap. Although high field magnetization measurements on single crystal samples of NENP and NINO have been done by us, the whole magnetization process until the saturation magnetization have not been observed because the exchange interaction J is still larger compared with the maximum field in our magnet.

Recently, another new Haldane gap material TMNIN: $(CH_3)_4NNi(NO_2)_3$ has been found by Renard *et al.*. [26] The crystal structure is similar to that of well-known one-dimensional antiferromagnet TMMC ($(CH_3)_4NMnCl_3$). Nickel ions are located along c-axis and they are bridged by three nitrite anions. The Ni-Ni distance is equal to $c/2=3.54$ Å. This bridging mode of the nitrite anions Ni-$(NO_2)_3$-Ni is quite different from the one in NENP and NINO which have the chain structure Ni-NO_2-Ni, as shown in the insert of Fig. 9. The chains are well separated by tetramethylammonium cations. Preliminary susceptibilty measurements show that the exchange parameter is small compared to NENP and NINO. The powdered sample is used for the magnetization measurements, and we can observe for the first time the whole magnetization process clearly by reducing the sample temperature below 1 K.

3. 2. 2. Experimental results

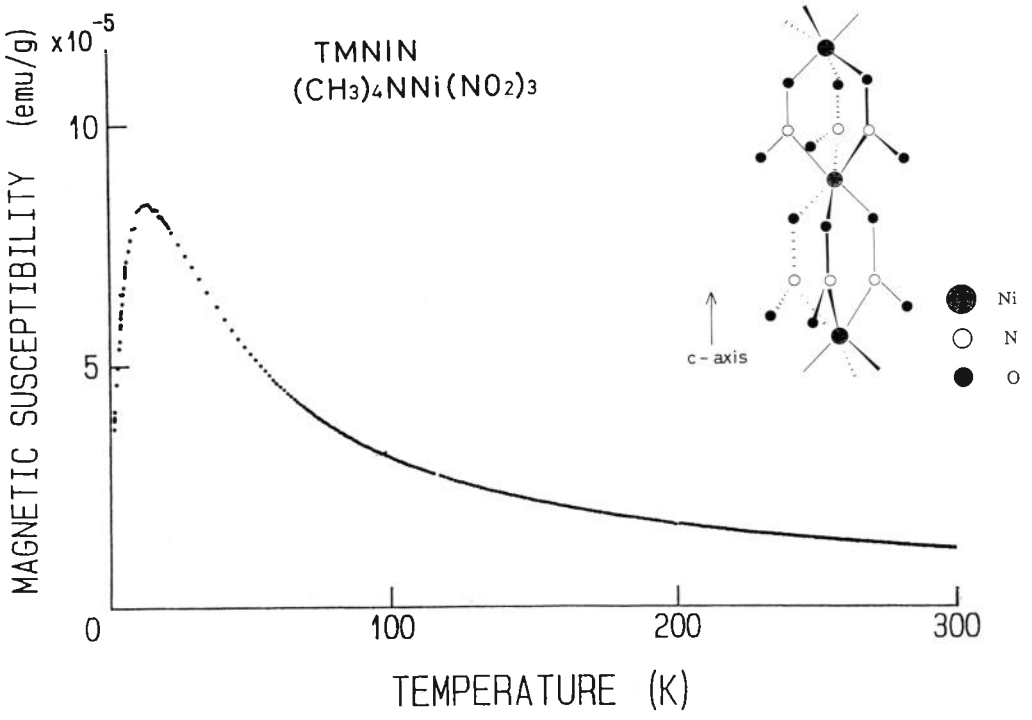

Fig. 9. Temperature dependence of the magnetic susceptibility in the powdered sample of TMNIN. Insert shows the chain structure of the specimen schematically.

Magnetic susceptiility datum of powdered sample of TMNIN is shown in Fig. 9. As expected for an antiferromagnetic chain system, the susceptibility increases as temperature decreases and shows a round maximum at about 15 K. At the low temperature region, the susceptibility decreases exponentially reflecting the existence of the gap. Above 20 K, the susceptibility is well understood by the orthodox model for the $S=1$ one-dimensional antiferromagnet with $J=-12$K and $g=2.25$. [26]

The high field magnetization curves of a powdered TMNIN up to 40 T at the lowest temperature of 0.55 K is shown in Fig. 10. The whole magnetization profile of TMNIN is similar to that of one-dimensional Heisenberg antiferromagnet with $S=1/2$ except for the low field region where TMNIN shows the clear evidence of the Haldane gap. The magnetic saturation is found above 30 T and the corresponding theoretical curve for $S=1$ one-dimensional Heisenberg antiferromagnet given by Parkinson and Bonner [27] is shown by a dotted line with the parameters of $|J|=12$ K and $g=2.25$. The agreement is satisfactory without the low field region where the theoretical calculation is not completed.

Magnetization curves up to 4 T at various temperatures are shown in Fig.11. The

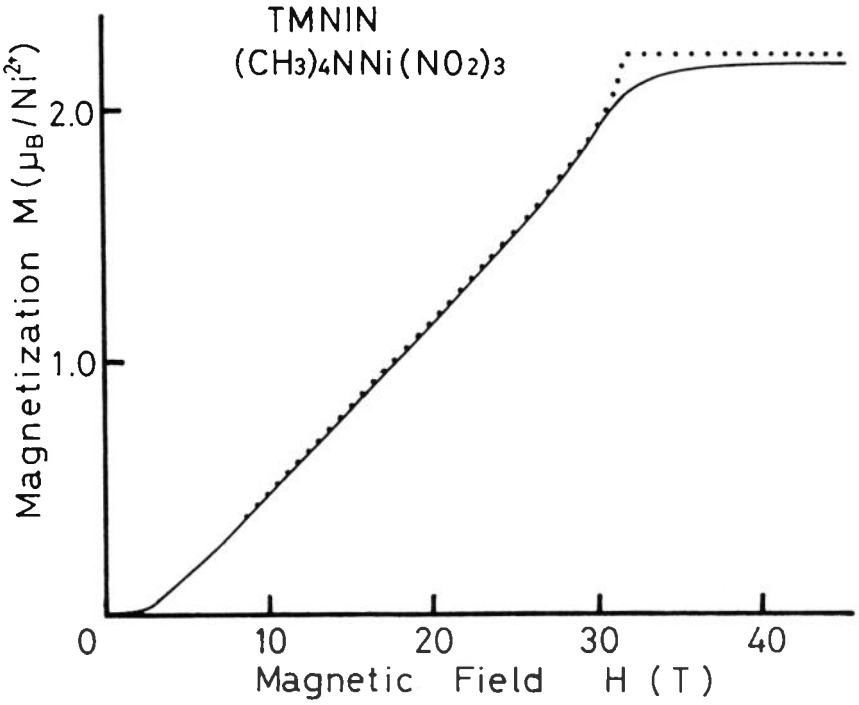

Fig.10. High field magnetization curve of TMNIN at 0.55 K. Dotted line shows the theoretical curve.

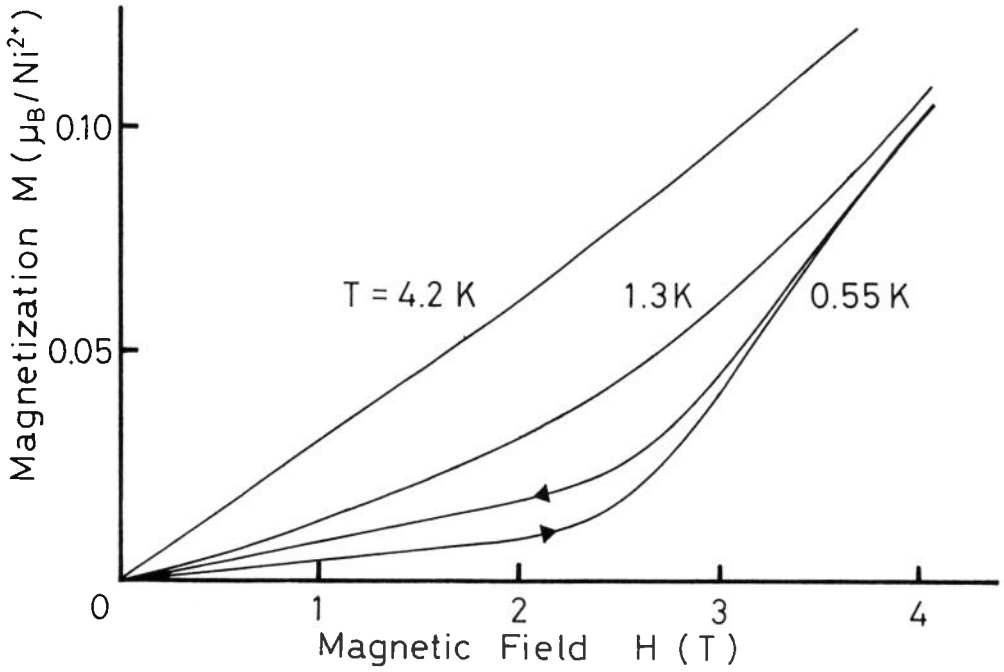

Fig. 11. Temperature dependences of magnetization in pulsed field up to 4 T.

magnetization is almost linear at 4.2 K but a clear change in the magnetization is found at 0.55 K. The magnetization profile at 0.55 K can be understood by the Haldane gap model same as in NENP and NINO. The sudden increase of magnetization around 2.5 T corresponds to the crossover from the nonmagnetic ground state to a sublevel of the excited

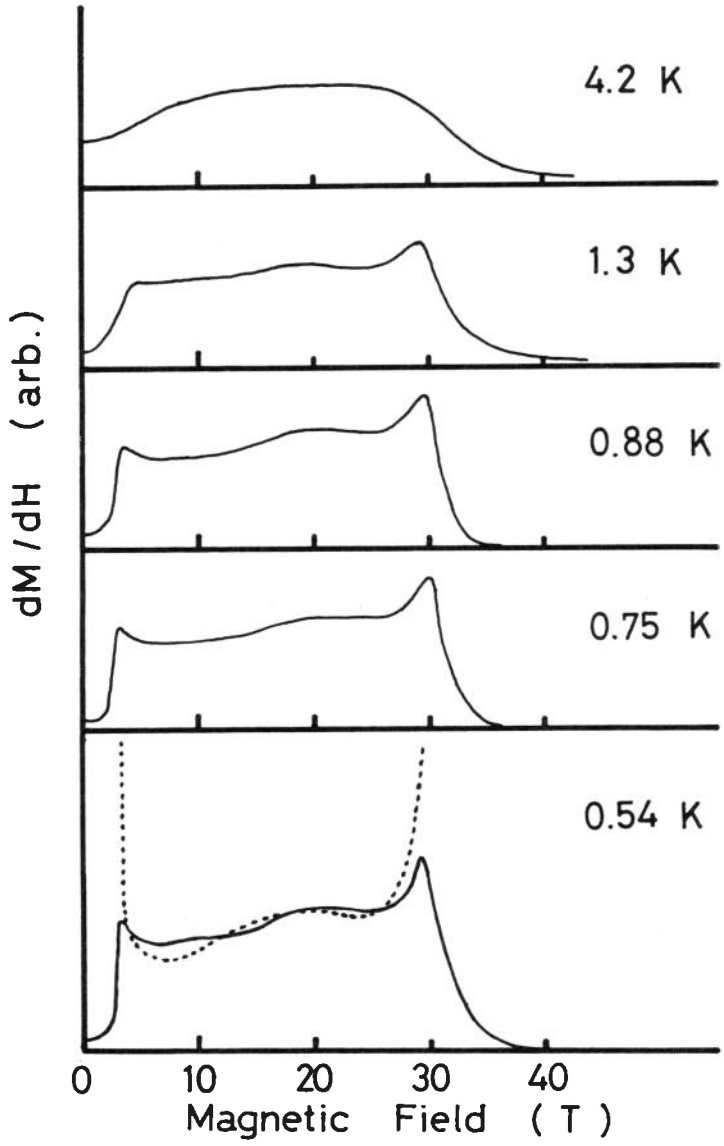

Fig.12. Temperature dependences of dM/dH of TMNIN. Dotted line is the theoretical curve given in ref. 28.

triplet.

The temperature dependence of the field derivative of magnetization curve dM/dH is shown in Fig. 12. Sakai and Takahashi [28] have done numerical diagonalizations up to $N=16$ on the $S=1$ one-dimensional Heisenberg antiferromagnet [28] and obtained the magnetization curve and the field derivative of magnetization curve dM/dH. The theoretical dM/dH curve is also shown in Fig. 12 by a dotted line, and is nicely in accord with the experimental curve. Therefore, it is concluded that TMNIN has the nature of ideal $S=1$ one-dimensional Heisenberg antiferromagnet. The transition field is defined as 2.7 T from the dM/dH curve and the corresponding energy gap E_g is estimated to be 4.1 K.

The obtained relations between the Haldane gap energy E_g and the intrachain exchange energy J is $E_g=0.34\,|J|$ in this compound. Collecting the results of the other various materials, [29] the relation is understood by the expression $E_g=(0.35\pm0.05)\,|J|$ which is close to the theoretical value of $E_g=0.41\,|J|$. [18] This confirms us that these materials are one-dimensional Heisenberg antiferromagnets and have the Haldane gap which is proportional to the intrachain exchange energy.

Acknowedgements

The authors wish to express their thanks to Prof. A. Yamagishl and Dr. T. Takeuchi of Research Center for Extreme Materials for helpful suggestions and assistances on use of plused magnets.

REFERENCES

[1] A. Yamagishl and M. Date: *High Field Magnetism*, ed. M. Date (North Holland, Amsterdam, 1983) p. 289.
[2] as a cumulative work, see, for example, *ibid.* and J. Magn. & Magn. Mater. (Netherlands), vol. **90 & 91**, (Conference Proceedings of "Magnetic Phase Transition" Nov. 1990).
[3] T. Yosida: *High Field Magnetism*, ed. M. Date (North Holland, Amsterdam, 1983) p. 305.
[4] T. Yosida, M. Morita and M. Date: J. Phys. Soc. Jpn. **57** (1988) 1428.
[5] T. Sakakibara, H. Mollymoto, M. Motokawa and M. Date: *High Field Magnetism*, ed. M. Date (North-Holland, Amsterdam, 1983), p. 299.
[6] T. Takeuchi, H. Hori, T. Yosida, A. Yamagishi, K. Katsumata, J. P. Renard, V. Gadet, M. Verdaguer and M. Date: J. Phys. Soc. Jpn. **61** (1992) 3262.
[7] S. C. Chang and G. A. Jeffrey: Acta Crystallogr. **B26** (1970) 673.
[8] K. J. Schenk and H. U. Güdel: Inorg. Chem. **21** (1982) 2253.
[9] L. A. Welo: Philos. Mag. ser. 7, **6** (1928) 481.
[10] K. Kambe: J. Phys. Soc. Jpn. **5** (1950) 48.

[11] L. Wucher and H. M. Gijsman: Physica **20** (1954) 361, 721.
[12] M. Morita and Y. Kato: Int. J. Quantum Chem. **18** (1980) 625.
[13] N. Uryû and S. A. Friedberg: Phys. Rev. **140** (1965) A1803.
[14] F. D. M. Haldane: Phys. Rev. Lett. **50** (1983) 1153.
[15] H. Bethe: Z. Phys. **71** (1931) 205.
[16] J. C. Bonner and M. E. Fisher: Phys. Rev. **A135** (1964) 640.
[17] I. Affleck, T. Kennedy, E. H. Lieb and H. Tasaki: Phys. Rev. Lett. **59** (1987) 799 and references therein.
[18] M. P. Nightingale and H. W. J. Blöte: Phys. Rev. **B33** (1986) 659.
[19] R. Botet, R. Jullien and M. Kolb: Phys. Rev. **B28** (1983) 3914.
[20] H. Tasaki: Phys. Rev. Lett. **64** (1990) 2066.
[21] W. J. L. Buyers, R. M. Morra, R. L. Armstrong, M. J. Hogan, P. Gerlach and K. Hirakawa: Phys. Rev. Lett. **56** (1986) 371.
[22] M. Steiner, K. Kakurai, J. K. Kjems, D. Petitgrand and R. Pynn: J. Appl. Phys. **61** (1987) 3953.
[23] J. P. Renard, M. Verdaguer, L. P. Regnault, W. A. C. Erkelens, J. Rossat-Mignod and W. G. Stirling: Europhys. Lett. **3** (1987) 945.
[24] J. P. Renard, M. Verdaguer, L. P. Regnault, W. A. C. Erkelens, J. Rossat-Mignod, J. Ribas, W. G. Stirling and C. Vettier: J. Appl. Phys. **63** (1988) 3538.
[25] M. Steiner, K. Kakurai, J. K. Kjems, D. Petitgrand and R. Pynn: J. Appl. Phys. **61** (1987) 3953.
[26] V. Gadet, M. Verdaguer, V. Briois, A. Gleizes, J. P. Renard, P. Beauvillain, C. Chappert, T. Goto, K. Le Dang and P. Veillet: Phys. Rev. **B44** (2) (1991) 705.
[27] J. B. Parkinson and J. C. Bonner: Phys. Rev. **B32** (1985) 4703.
[28] T. Sakai and M. Takahashi: Phys. Rev. **B43** (1991) 13383.
[29] T. Takeuchi, H. Hori, M. Date, A. Yamagishi, T. Yosida, K. Katsumata, J. P. Renard, V. Gadet and M. J. Verdaguer: J. Magn. & Magn. Mater. (Netherlands), **104-107** (1992) 813.